

September 2012

# Hidden sector dark matter explains the DAMA, CoGeNT and CRESST-II experiments

R. Foot<sup>1</sup>

*ARC Centre of Excellence for Particle Physics at the Terascale,  
School of Physics, University of Melbourne,  
Victoria 3010 Australia*

We examine data from the DAMA, CoGeNT and CRESST-II direct detection experiments in the context of multi-component hidden sector dark matter. The models considered feature a hidden sector with two or more stable particles charged under an unbroken  $U(1)'$  gauge interaction. The new gauge field can interact with the standard  $U(1)_Y$  via renormalizable kinetic mixing, leading to Rutherford-type elastic scattering of the dark matter particles off ordinary nuclei. We consider in detail the simplest generic model of this type, with a hidden sector composed of two stable particles,  $F_1$  and  $F_2$ . We find that this simple model can simultaneously explain the DAMA, CoGeNT and CRESST-II data. This explanation is consistent with the null results of CDMS/Si and CDMS/Ge but has some tension with the most recent results from the XENON100 experiment.

---

<sup>1</sup>E-mail address: rfoot@unimelb.edu.au

# 1 Introduction

The existence of a new type of matter, non-baryonic dark matter, is clearly indicated by observations on small and large astronomical scales. In particular, the observed flat rotation curves in spiral galaxies, CMB anisotropies, and matter power spectrum suggest the existence of a cold (or warm) dark matter component with energy density around five times larger than ordinary baryons[1]. These inferences aside, the precise nature of dark matter is not yet known. If dark matter interacts with ordinary matter then it might be directly detectable with Earth based experiments, some of which have yielded some impressive results. Most notable, are the DAMA/NaI [2] and DAMA/LIBRA [3] experiments. These experiments have observed an annual modulation in the ‘single hit’ event rate, over more than 12 annual cycles, with phase consistent with expectations from dark matter interactions[4]. Over the last few years, the CoGeNT experiment[5, 6], using a p-type point-contact Germanium detector with very low energy threshold, has observed a rising event rate at low energies. These events could not be explained by known backgrounds and provide evidence supporting the DAMA signal. Most recently, the CRESST-II collaboration[7] have obtained results that cannot be explained by known backgrounds and are compatible with a dark matter signal also rising at low energies.

A satisfactory explanation of these experiments requires a specific model for dark matter. One promising approach appears to be in the framework of multi-component hidden sector dark matter[8, 9, 10, 11, 12]. In this scenario dark matter arises from a multi-component hidden sector which contains an unbroken  $U(1)'$  gauge interaction. The new gauge field is presumed to interact with the standard  $U(1)_Y$  via renormalizable kinetic mixing, leading to Rutherford-type elastic scattering of the dark matter particles off ordinary nuclei. The specific case where the hidden sector is isomorphic to the ordinary sector, mirror dark matter[13, 14], has also been discussed at length, and found to be compatible with the DAMA, CoGeNT and CRESST-II results[12] (see also [8, 9, 11]). More generally, though, these works indicate that there is a large class of such hidden sector dark matter models which are compatible with the experiments. The purpose of this article is to examine in detail the simplest such multi-component hidden sector dark matter model. It serves as a useful prototype of generic multi-component dark matter models of this kind.

The outline of this article is as follows. In section 2 we review some general aspects of the considered hidden sector dark matter framework. In section 3 we look at the specific case of the model with two stable hidden sector particles,  $F_1$  and  $F_2$ . In section 4 we confront this two component hidden sector model with the latest data from DAMA, CoGeNT and CRESST-II experiments. In section 5, we follow up on an example near the combined best fit identified in section 4. In section 6, we examine the compatibility of this example with CDMS and XENON100 data. Finally, in section 7 we conclude.

## 2 Hidden sector dark matter

The models we consider relegate dark matter particles to a generic hidden sector with an unbroken  $U(1)'$  gauge interaction. The special case where the hidden sector is isomorphic to the standard model sector - mirror dark matter - has been discussed in the context of direct detection experiments in ref.[8, 9, 11, 12]. Here we consider the more generic hidden sector case. This includes models with broken mirror symmetry[15] and many other hidden sector models[16]. More generally, hidden sector models with light stable particles can also be motivated from the similar inferred energy density of ordinary and dark matter in the Universe[17].

In this paper we consider spin-independent elastic scattering of dark matter particles on ordinary nuclei. The dark matter particles are assumed to arise from a hidden sector which contains an unbroken  $U(1)'$  gauge interaction and possibly other gauge interactions. This means that the interactions of the theory are described by the Lagrangian:

$$\mathcal{L} = \mathcal{L}_{SM}(e, \nu, u, d, B_\mu, \dots) + \mathcal{L}_{dark}(F_1, F_2, \dots, F_N, B'_\mu, \dots) + \mathcal{L}_{mix} \quad (1)$$

where  $\mathcal{L}_{mix}$  contains possible interactions connecting ordinary and hidden sector particles. An example of  $\mathcal{L}_{dark}$ , with  $N$  Dirac fermions  $F_j$ ,  $j = 1, \dots, N$ , is

$$\mathcal{L}_{dark} = -\frac{1}{4}F'_{\mu\nu}F'^{\mu\nu} + \bar{F}_j (iD_\mu \gamma^\mu - m_j) F_j \quad (2)$$

where  $D_\mu = \partial_\mu + ig'B'_\mu Q'$  is the covariant derivative and  $j$  is summed over  $1, \dots, N$ . In this example the  $N$  particles  $F_j$  are each absolutely stable due to the presence of  $U(1)_1 \otimes U(1)_2 \otimes \dots \otimes U(1)_N$  global symmetries. Importantly these symmetries are not imposed; they are accidental, like the  $U(1)_B$  and  $U(1)_L$  global symmetries of the standard model. Evidently, having dark matter arise from a hidden sector is theoretically attractive because it is a natural way to introduce dark matter particles which are dark, massive, stable and importantly do not modify standard model physics.

Dark matter elastic scattering depends on the cross-section,  $d\sigma/dE_R$ , and on the halo distribution function,  $f_{F_j}$ , of the dark matter species (taking the general case of  $N$  stable species). Both of these quantities depend crucially on the particle physics. Considering first the cross-section, this can have different recoil energy dependence depending on the type of interaction. The most common form considered in the literature is contact interactions which give an energy independent cross-section (excepting here the energy dependence due to the form factor). However, we consider Rutherford scattering which features non-trivial energy dependence,  $d\sigma/dE_R \propto 1/E_R^2$ [8]. From the point of view of hidden sector dark matter, where the hidden sector contains an unbroken  $U(1)'$  gauge interaction, the latter appears to be the most natural form of interaction since it arises from  $U(1)' - U(1)_Y$  renormalizable kinetic mixing. Rutherford scattering results because the interaction is mediated by a massless particle (the photon).<sup>2</sup>

---

<sup>2</sup>The case where the mediator is light is also possible, and has been studied recently in ref.[18]. As discussed there, in the context of the DAMA, CoGeNT and CRESST-II experiments, Rutherford scattering arises if the mediator has mass much less than 10 MeV, while point-like interaction arises if the mediator has mass much greater than 10 MeV.

The distribution function,  $f_{F_j}$ , also depends on the particle physics. For dark matter composed of only one type of particle with mass,  $m$ , the distribution is typically assumed to be Maxwellian, with an effective temperature set by the galactic rotational velocity:  $T = \frac{1}{2}mv_{rot}^2$ . This leads to a distribution:  $f = \exp(-v^2/v_0^2)$  with  $v_0 = v_{rot}$ . On the other hand, if dark matter is multi-component and self-interacting both plausible if dark matter arises from a hidden sector with unbroken  $U(1)'$  gauge interaction, then the distribution function is still Maxwellian, but the velocity dispersion depends on the mass of the species. Since  $f_{F_j} = \exp(-E/T) = \exp(-\frac{1}{2}m_j v^2/T)$ , it follows that  $v_0[F_j] = \sqrt{2T/m_j}$  (recall the index  $j$  labels the stable particle species,  $j = 1, \dots, N$ ). If the interactions are frequent enough so that the particles in the halo have a common (local) temperature,  $T$ , then it follows that the velocity dispersion depends on  $m_j$  via  $v_0[F_j] \propto 1/\sqrt{m_j}$ . In fact assuming an isothermal pressure supported halo in hydrostatic equilibrium, one can show that[9]

$$v_0[F_j] = v_{rot} \sqrt{\frac{\bar{m}}{m_j}} \quad (3)$$

where  $\bar{m} = \sum n_j m_j / \sum n_j$  is the mean mass of the particles in the halo. Thus the velocity dispersion can vary greatly depending on the masses within the model.

### 3 Two component hidden sector dark matter

Consider the case where the hidden sector contains two stable  $U(1)'$  charged dark matter particles  $F_1$  and  $F_2$  with masses  $m_{F_1}$  and  $m_{F_2}$  [ $F_1$  and  $F_2$  can be fermionic as in the example Eq.(2) or alternatively bosonic]. If their abundance in the Universe arises from a particle-antiparticle asymmetry then two stable particles with opposite in sign, but not necessarily equal in magnitude,  $Q'$  charges is actually the minimal case given  $Q'$  neutrality of the Universe. In fact this neutrality is not just global,  $U(1)'$  electric fields will ensure local neutrality of a plasma containing  $F_1$  and  $F_2$  particles. That is,

$$n_{F_1} Q'_{F_1} + n_{F_2} Q'_{F_2} = 0 \quad (4)$$

where  $n_{F_j}$  [ $Q'_{F_j}$ ] is the local number density [ $U(1)'$  charge] of  $F_j$ .

We assume that the  $U(1)'$  gauge field interacts with the standard  $U(1)_Y$  gauge field via renormalizable kinetic mixing interaction[19]:

$$\mathcal{L}_{mix} = \frac{\epsilon'}{2 \cos \theta_w} F^{\mu\nu} F'_{\mu\nu} \quad (5)$$

where  $F_{\mu\nu}$  is the standard  $U(1)_Y$  gauge boson field strength tensor, and  $F'_{\mu\nu}$  is the field strength tensor for the hidden sector  $U(1)'$ . This interaction enables the hidden sector  $U(1)'$  charged particles  $F_j$  to couple to ordinary photons[20] with electric charge  $g' Q'_{F_j} \epsilon' \equiv \epsilon_{F_j} e$ . [Henceforth we define  $\epsilon \equiv \epsilon_{F_2}$ ]. The cross-section of a  $F_2$  particle to elastically scatter off an ordinary nucleus,  $A$ , presumed at rest with atomic number  $Z$ ,

is given by[8]:<sup>3</sup>

$$\frac{d\sigma}{dE_R} = \frac{\lambda}{E_R^2 v^2} \quad (6)$$

where

$$\lambda \equiv \frac{2\pi\epsilon^2 Z^2 \alpha^2}{m_A} F_A^2(qr_A) \quad (7)$$

and  $F_A(qr_A)$  is the form factor which takes into account the finite size of the nuclei. A simple analytic expression for the form factor, which we adopt in our numerical work, is the one proposed by Helm[21, 22].

To explain the rotation curves in spiral galaxies, we assume that the  $F_1$  and  $F_2$  particles are (roughly) spherically distributed in galaxies in a pressure supported halo [c.f. ref.[23]]. We assume that the self-interactions are frequent enough as to thermalize the distributions of  $F_1$  and  $F_2$  with a common temperature  $T$ . We further assume that the binding energy of atomic bound states containing  $F_1$  and  $F_2$  particles are much less than this temperature, so that the  $F_1$  and  $F_2$  particles can be treated as two components of a plasma<sup>4</sup>. Typically this requires  $\alpha'^2 m_{F_1} m_{F_2} / (m_{F_1} + m_{F_2}) \ll \text{keV}$  where  $\alpha' \equiv g'^2 Q'_{F_1} Q'_{F_2} / 4\pi$ .

As mentioned earlier, the condition of hydrostatic equilibrium relates the temperature of the particles to the galactic rotational velocity,  $v_{rot}$ , resulting in a mass dependent velocity dispersion, Eq.(3). In the two component case the mean mass of the particles in the galactic halo is given by

$$\begin{aligned} \bar{m} &\equiv \frac{n_{F_1} m_{F_1} + n_{F_2} m_{F_2}}{n_{F_1} + n_{F_2}} \\ &= \frac{m_{F_1} - \frac{Q'_{F_1}}{Q'_{F_2}} m_{F_2}}{1 - \frac{Q'_{F_1}}{Q'_{F_2}}} \end{aligned} \quad (8)$$

where we have made use of Eq.(4). The interesting region of parameter space, from the point of view of direct detection experiments, is where  $m_{F_1} \ll m_{F_2}$  and  $|Q'_{F_1}| \ll |Q'_{F_2}|$  so that  $\bar{m} \ll m_{F_2}$ . It then follows from Eq.(3) that  $v_0^2(F_2) \ll v_{rot}^2$ . The narrow velocity dispersion (recall  $\sigma_v^2 = 3v_0^2/2$ ) can greatly reduce the rate of  $F_2$  interactions in higher threshold experiments such as XENON100[25] and CDMS/Ge [26] whilst still allowing  $F_2$  to explain the signals in the lower threshold DAMA and CoGeNT experiments. The  $F_1$  state can be too light to be directly detected in the experiments (roughly this means that  $m_{F_1} \lesssim 5 \text{ GeV}$ ), but influences the way  $F_2$  interacts due to its effect on the velocity dispersion of  $F_2$ . With these assumptions, current experiments depend on three

---

<sup>3</sup>Unless otherwise indicated, we employ natural units where  $\hbar = c = 1$ .

<sup>4</sup>The alternative case, where  $F_1$  and  $F_2$  are tightly bound into atoms has been discussed recently in ref.[24]. In the tightly bound limit, the interaction between ordinary matter and such atomic dark matter becomes point-like, and its implications for direct detection experiments are quite different from the case we discuss here.

parameters,  $m_{F_2}$ ,  $\bar{m}$ ,  $\epsilon\sqrt{\xi_{F_2}}$  (the parameter,  $\xi_{F_2}$  will be defined in a moment). This two component hidden sector dark matter model has been briefly discussed previously in ref.[11]. Our purpose here is to study it in more detail taking into account the tentative dark matter signal coming from the CRESST-II experiment[7] as well as the updated results from CoGeNT[6].

The differential scattering rate for  $F_j$  on a target nuclei,  $A$ , is given by<sup>5</sup>:

$$\frac{dR}{dE_R} = N_T n_{F_j} \int_{|\mathbf{v}| > v_{min}}^{\infty} \frac{d\sigma}{dE_R} \frac{f_{F_j}(\mathbf{v}, \mathbf{v}_E)}{k} |\mathbf{v}| d^3v \quad (9)$$

where the integration limit,  $v_{min}$ , is defined by the kinematic relation:

$$v_{min} = \sqrt{\frac{(m_A + m_{F_j})^2 E_R}{2m_A m_{F_j}^2}}. \quad (10)$$

In Eq.(9),  $N_T$  is the number of target nuclei per kg of detector and  $n_{F_j}$  is the number density of the halo dark matter particles  $F_j$  at the Earth's location. This number density can be expressed in terms of the halo mass fraction of  $F_j$ ,  $\xi_{F_j}$ , and total mass density,  $\rho_{dm}$  via  $n_{F_j} = \rho_{dm} \xi_{F_j} / m_{F_j}$  (we set  $\rho_{dm} = 0.3 \text{ GeV/cm}^3$ ). Also in Eq.(9)  $\mathbf{v}$  denotes the velocity of the halo particles relative to the Earth and  $\mathbf{v}_E$  the velocity of the Earth relative to the galactic halo<sup>6</sup>. The halo distribution function, in the reference frame of the Earth, is then given by the Maxwellian distribution:

$$\frac{f_{F_j}(\mathbf{v}, \mathbf{v}_E)}{k} = (\pi v_0^2 [F_j])^{-3/2} \exp\left(\frac{-(\mathbf{v} + \mathbf{v}_E)^2}{v_0^2 [F_j]}\right). \quad (11)$$

The integral, Eq.(9), can be simplified in terms of error functions[10, 22] and solved numerically.

Detector resolution effects can be incorporated by convolving the rate with a Gaussian:

$$\frac{dR}{dE_R^m} = \frac{1}{\sqrt{2\pi}\sigma_{res}} \int \frac{dR}{dE_R} e^{-(E_R - E_R^m)^2 / 2\sigma_{res}^2} dE_R \quad (12)$$

where  $E_R^m$  is the measured energy and  $\sigma_{res}$  defines the resolution. The unit of measured energy is often in keVee units (ionization/scintillation energy). For nuclear recoils, without channeling, keVee = keV/ $q$ , where  $q < 1$  is the relevant quenching factor. Channeled events, where scattered target atoms travel down the axis and planes of the target crystal, have  $q \simeq 1$ . In view of the theoretical study[27], we assume that the channelled fraction is negligible. Of course channeling may involve subtleties and the modeling used in ref.[27] might have missed important effects. Hence it is, of course, still conceivable that channeling could play an important role, which could perhaps modify the favored regions of parameter space.

<sup>5</sup>The upper limit of integration in Eq.(9) is taken as infinity since we are dealing with dark matter particles with potentially significant self-interactions. The self-interactions can prevent particles in the high velocity tail of the Maxwellian distribution from escaping the galaxy.

<sup>6</sup>In all numerical work we include an estimate of the Sun's peculiar velocity so that  $\langle |\mathbf{v}_E| \rangle = v_{rot} + 12 \text{ km/s}$ .

Bin / keV	Total events	Estimated background
10.2 – 13.0	9	3.2
13 – 16	15	6.1
16 – 19	11	7.0
19 – 25	12	11.5
25 – 40	20	20.1

Table 1: CRESST-II data: total number of events and estimated background.

## 4 Direct detection of hidden sector dark matter

As discussed earlier, the two component hidden sector model supposes dark matter arises from a hidden sector with two components  $F_1$  and  $F_2$ . With  $m_{F_1} \lesssim 5$  GeV, the existing direct detection experiments depend on three parameters:  $m_{F_2}$ ,  $\epsilon\sqrt{\xi_{F_2}}$ ,  $\bar{m}$ . It was shown in ref.[11] that with  $\bar{m} = 1$  GeV and  $v_{rot} = 240$  km/s (fixed as a specific example) this model could provide a reasonable fit to the DAMA annual modulation signal and measured CoGeNT spectrum. Since that time, the measured CoGeNT spectrum has undergone a significant ‘surface event correction’[6]. Additionally, CRESST-II have announced results suggesting a tentative dark matter signal. Our purpose now is to re-examine the two component hidden sector model in light of these new experimental developments. We shall also extend our previous analysis by considering a wider range of  $\bar{m}$ ,  $v_{rot}$  values. In particular we consider  $\bar{m}/\text{GeV} = 1.0$  and  $3.0$  and two values for the rotational velocity,  $v_{rot} = 200$  km/s and  $v_{rot} = 240$  km/s. Although  $v_{rot} = 240$  km/s is representative of recent measurements of the local rotational velocity of the Milky Way[28] there are significant uncertainties in this quantity and it is useful to see how things change when  $v_{rot}$  is varied.

### *The CRESST-II experiment*

The CRESST-II experiment has collected a 730 kg-day exposure using a  $\text{CaWO}_4$  target[7]. The data arises from 8 detector modules, with recoil energy thresholds (keV) of 10.2, 12.1, 12.3, 12.9, 15.0, 15.5, 16.2, 19.0. With a view to performing a standard  $\chi^2$  analysis, we bin this data into 5 bins, summarized in table 1. This table also includes the expected background rate[7] (see also [29]).

For the CRESST-II analysis, we define  $\chi^2$  in the standard way:

$$\chi^2(m_{F_2}, \epsilon\sqrt{\xi_{F_2}}, \bar{m}) = \sum_{i=1}^5 \left[ \frac{R_i + B_i - \text{data}_i}{\delta \text{data}_i} \right]^2 \quad (13)$$

where  $R_i$  is the theoretically predicted rate and  $B_i$  is the estimated background in the  $i^{th}$  energy bin. The relevant rates,  $R_i$ , for the CRESST-II experiment are computed using Eq.(9) and Eq.(12). We use  $\sigma_{res} = 0.3$  keV[7] and assume detection efficiencies,  $\epsilon_f$ , for the three target elements:  $\epsilon_f = 0.9$  for  $O, W$  and  $\epsilon_f = 1.0$  for  $Ca$ , which take into account their acceptance region. We have not assumed any uncertainty in the CRESST-II energy scale.

### *The DAMA experiment*

The DAMA/NaI and DAMA/LIBRA experiments have accumulated data from a large exposure [1.17 ton-year] using a *NaI* target[2, 3]. Analysis of this data has yielded an annual modulation with phase consistent with dark matter expectations at around  $8.9\sigma$  C.L. We analyse this annual modulation signal in the energy range  $2 - 8$  keVee using 12 bins of width 0.5 keVee[3]. The detector resolution, obtained from ref.[30], has been included. An important issue is the nuclear recoil energy scale which is set by the values of the quenching factors  $q_{Na}$ ,  $q_I$ . Following our mirror dark matter analysis[12], we consider a range of possible values for the quenching factors:

$$q_{Na} = 0.28 \pm 0.08, \quad q_I = 0.12 \pm 0.08 . \quad (14)$$

We minimize  $\chi^2$  varying  $q_{Na}$ ,  $q_I$  over the above range of values (assumed energy independent for simplicity). Values of  $q_I$ ,  $q_{Na}$  outside the above range are possible and have been discussed in the literature. For example, the higher values  $q_{Na} \approx 0.6$ ,  $q_I \approx 0.3$  have been suggested by Tretyak[31]. Although the possibility of such high quenching factors are not specifically considered in our numerical work, qualitatively, we can say that higher quenching factors generally move the DAMA allowed region to lower values of  $\epsilon\sqrt{\xi_{F_2}}$ ,  $m_{F_2}$  and also leads to interesting parameter space overlapping with that from CoGeNT and CRESST-II.

### *The CoGeNT experiment*

The CoGeNT collaboration has recently presented data corresponding to an exposure of  $0.33 \times 807$  kg-days in a Germanium target[6]. This update of their earlier exposure[5] includes an important correction for surface events which have not been excluded by their rise time cut[6]. We take the efficiency corrected and surface event corrected CoGeNT data from figure 21 of ref.[6]. We analyse this data using 15 bins of width 0.1 keVee in the region  $0.5 - 2.0$  keVee. We allow for a constant background, which we fit to the data in this energy range. We have taken into account some uncertainties in energy scale by minimizing the  $\chi^2$  for CoGeNT over the variation in quenching factor,  $q_{Ge} = 0.21 \pm 0.04$ .

### *The analysis*

We summarize the  $\chi^2(min)$  values for the relevant data sets from each experiment for the two considered  $\bar{m}$  values in table 2 for  $v_{rot} = 200$  km/s and table 3 for  $v_{rot} = 240$  km/s.

The  $2\sigma$  ( $3\sigma$ ) favored region of parameter space is bounded by the contours where  $\chi^2(m_{F_2}, \epsilon\sqrt{\xi_{F_2}}) = \chi_{min}^2 + 4(9)$ . In figure 1 we plot the CRESST-II  $2\sigma$  favored region along with the  $3\sigma$  favored region of parameter space for DAMA and CoGeNT for  $v_{rot} = 200$  km/s and with reference value of  $\bar{m}$ :  $\bar{m} = 1.0$  GeV (figure 1a),  $\bar{m} = 3.0$  GeV (figure 1b). In figure 2 we repeat the exercise, but with  $v_{rot} = 240$  km/s.



Experiment	$\chi^2(min)/d.o.f.$	$\bar{m}/\text{GeV}$	Best fit parameters
DAMA (annual mod.)	5.8/10	$\bar{m} = 1.0$	$m_{F_2} = 56.0 \text{ GeV}, \epsilon\sqrt{\xi_{F_2}} = 7.2 \times 10^{-9}$
CoGeNT (spectrum)	9.4/12	$\bar{m} = 1.0$	$m_{F_2} = 36.0 \text{ GeV}, \epsilon\sqrt{\xi_{F_2}} = 4.9 \times 10^{-9}$
CRESST (spectrum)	0.1/3	$\bar{m} = 1.0$	$m_{F_2} = 80.0 \text{ GeV}, \epsilon\sqrt{\xi_{F_2}} = 4.9 \times 10^{-9}$
DAMA (annual mod.)	6.1/10	$\bar{m} = 3.0$	$m_{F_2} = 58.0 \text{ GeV}, \epsilon\sqrt{\xi_{F_2}} = 7.8 \times 10^{-9}$
CoGeNT (spectrum)	10.5/12	$\bar{m} = 3.0$	$m_{F_2} = 44.0 \text{ GeV}, \epsilon\sqrt{\xi_{F_2}} = 5.5 \times 10^{-9}$
CRESST (spectrum)	0.3/3	$\bar{m} = 3.0$	$m_{F_2} = 74.0 \text{ GeV}, \epsilon\sqrt{\xi_{F_2}} = 5.0 \times 10^{-9}$

Table 2: Summary of  $\chi^2(min)$  for the relevant data sets from the DAMA, CoGeNT and CRESST-II experiments for two reference  $\bar{m}$  values and  $v_{rot} = 200 \text{ km/s}$ .

Experiment	$\chi^2(min)/d.o.f.$	$\bar{m}/\text{GeV}$	Best fit parameters
DAMA (annual mod.)	5.0/10	$\bar{m} = 1.0$	$m_{F_2} = 42.0 \text{ GeV}, \epsilon\sqrt{\xi_{F_2}} = 7.4 \times 10^{-9}$
CoGeNT (spectrum)	9.7/12	$\bar{m} = 1.0$	$m_{F_2} = 28.5 \text{ GeV}, \epsilon\sqrt{\xi_{F_2}} = 4.7 \times 10^{-9}$
CRESST (spectrum)	0.2/3	$\bar{m} = 1.0$	$m_{F_2} = 57.7 \text{ GeV}, \epsilon\sqrt{\xi_{F_2}} = 4.1 \times 10^{-9}$
DAMA (annual mod.)	6.1/10	$\bar{m} = 3.0$	$m_{F_2} = 46.0 \text{ GeV}, \epsilon\sqrt{\xi_{F_2}} = 9.2 \times 10^{-9}$
CoGeNT (spectrum)	10.7/12	$\bar{m} = 3.0$	$m_{F_2} = 36.5 \text{ GeV}, \epsilon\sqrt{\xi_{F_2}} = 5.5 \times 10^{-9}$
CRESST (spectrum)	0.4/3	$\bar{m} = 3.0$	$m_{F_2} = 39.8 \text{ GeV}, \epsilon\sqrt{\xi_{F_2}} = 4.9 \times 10^{-9}$

Table 3: Summary of  $\chi^2(min)$  for the relevant data sets from the DAMA, CoGeNT and CRESST-II experiments for two reference  $\bar{m}$  values and  $v_{rot} = 240 \text{ km/s}$ .

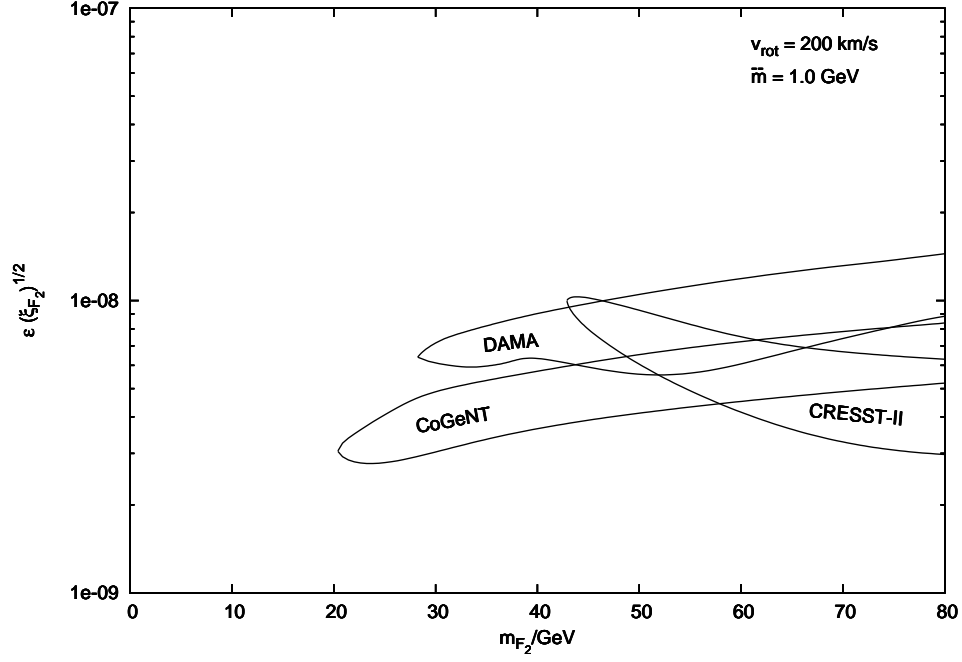


Figure 1a: DAMA, CoGeNT and CRESST-II favored regions of parameter space in the two component hidden sector model. The reference point  $v_{\text{rot}} = 200 \text{ km/s}$  and  $\bar{m} = 1.0 \text{ GeV}$  is assumed.

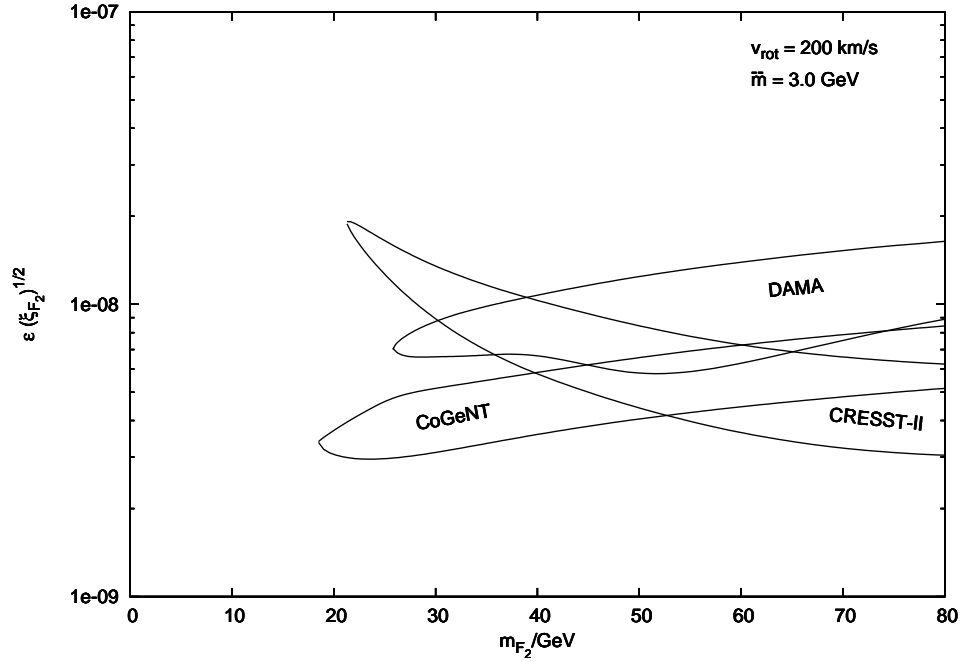


Figure 1b: Same as figure 1a, except that  $\bar{m} = 3.0 \text{ GeV}$  is assumed.

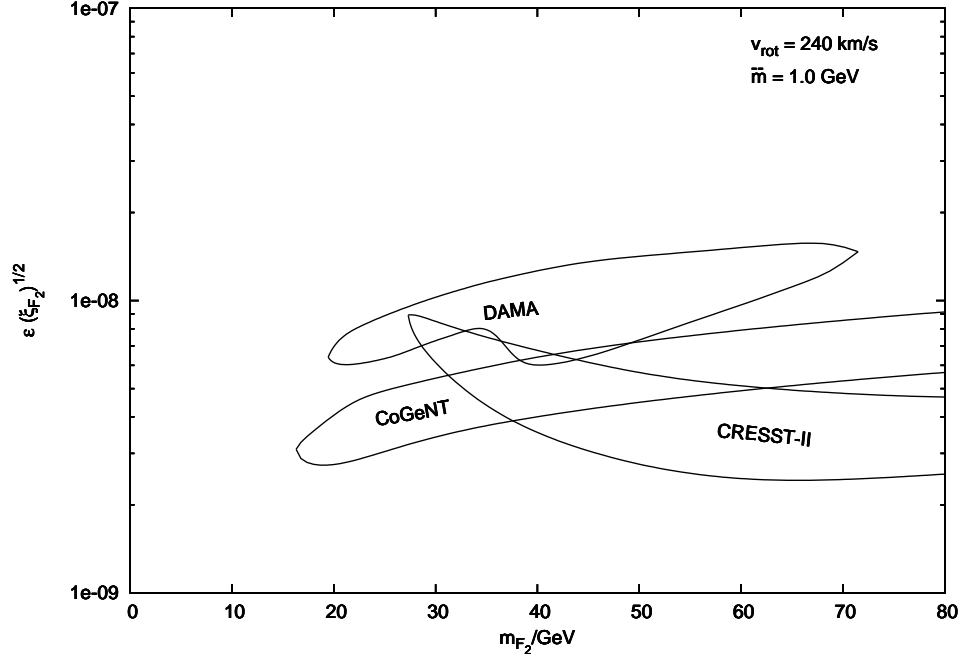


Figure 2a: DAMA, CoGeNT and CRESST-II favored regions of parameter space in the two component hidden sector model. The reference point  $v_{\text{rot}} = 240 \text{ km/s}$  and  $\bar{m} = 1.0 \text{ GeV}$  is assumed.

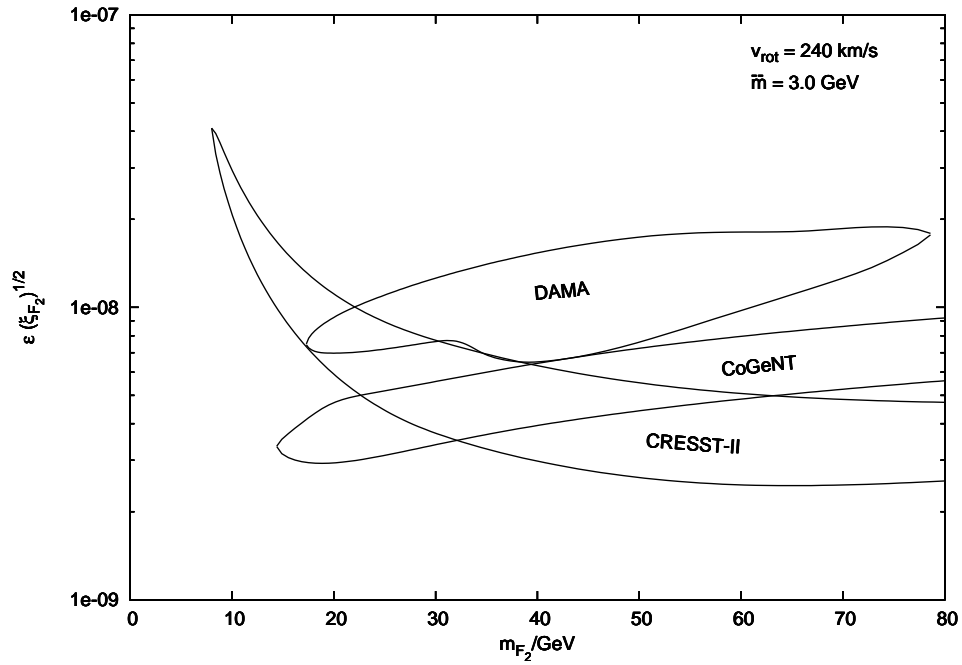


Figure 2b: Same as figure 2a, except that  $\bar{m} = 3.0 \text{ GeV}$  is assumed.

The figures demonstrate that there are quite large regions of parameter space where each experiment can be explained within this hidden sector framework. For DAMA, the signal is dominated by  $F_2 - Na$  scattering if  $m_{F_2} \lesssim 40$  GeV, while if  $m_{F_2} \gtrsim 40$  GeV then both  $F_2 - Na$  and  $F_2 - I$  scattering conspire to produce the signal. Also, the signal arises from scattering of target nuclei with  $F_2$  particles from the body of their Maxwellian halo distribution (rather than, say, the tail) and thus is reasonably stable, and shows little dependence on the velocity dispersion i.e. on  $\bar{m}$ .

For CoGeNT, the spectrum is consistent with  $dR/dE_R \propto 1/E_R^2$ , predicted from the energy dependence of the Rutherford cross section. This is the reason why the CoGeNT spectrum is reproduced for a large range of  $F_2$  mass. In other words, the shape of the CoGeNT spectrum arises from dynamics rather than kinematic effects in this model. Again there is little dependence on the  $\bar{m}$  parameter.

Finally, in the case of CRESST-II, the dominant signal contribution arises from  $F_2 - Ca$  scattering for  $m_{F_2} \sim 50$  GeV. For such masses,  $F_2$  particles in the body of their Maxwellian halo distribution can scatter to produce nuclear recoils above the 10 keV threshold. As the mass of  $F_2$  is lowered,  $m_{F_2} \lesssim 40 - 50$  GeV, a recoil above threshold can only occur for  $F_2$  particles in the tail of the Maxwellian halo distribution. For this reason, there is quite a bit of dependence of the CRESST-II allowed region on the velocity dispersion, i.e.  $\bar{m}$  in this mass range.

The figures show that the allowed region of parameters favoured by DAMA, CoGeNT and CRESST-II are very similar with some degree of overlap. This occurs ignoring a variety of possible systematic effects, such as the possibility of channeled events in DAMA (which can lower the DAMA favoured values of  $\epsilon\sqrt{\xi_{F_2}}$ ), and uncertainties in the surface event correction factor for CoGeNT (which could raise or lower the CoGeNT favoured values of  $\epsilon\sqrt{\xi_{F_2}}$ ). Thus realistically there is quite a large region of parameter space that is possible, much larger than the overlapping allowed region, even assuming all three experiments have detected dark matter interactions. It is difficult, though, to quantify all the possible systematic effects and do an exhaustive analysis. Instead, we shall hope to gain some insight by examining a particular point in parameter space.

## 5 An example near the combined best fit of DAMA, CoGeNT and CRESST-II

In view of potential systematic uncertainties between the experiments we shall resist the temptation to fit the combined DAMA, CoGeNT and CRESST-II data. Instead we shall consider an example reference point  $P1$  located near the overlapping allowed regions indicated in figure 1a.

$$P1 : m_{F_2} = 50 \text{ GeV}, \epsilon\sqrt{\xi_{F_2}} = 5.7 \times 10^{-9}, \bar{m} = 1.0 \text{ GeV}, v_{rot} = 200 \text{ km/s} \quad (15)$$

The DAMA annual modulation signal for this example is given in figure 3a, the CoGeNT spectrum in figure 3b, and CRESST-II spectrum in figure 3c.

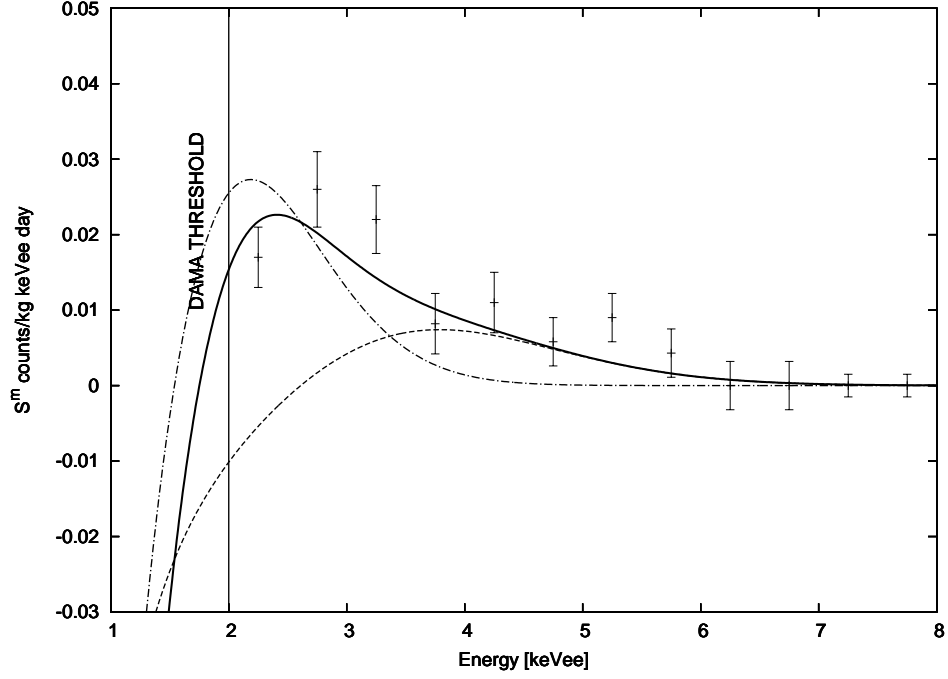


Figure 3a: DAMA annual modulation spectrum for two component hidden sector dark matter with parameters  $P1$  (solid line). The separate contributions from scattering off sodium (dotted line) and Iodine (dashed-dotted line) are also shown. In this example  $q_{Na} = 0.36$ ,  $q_I = 0.20$ .

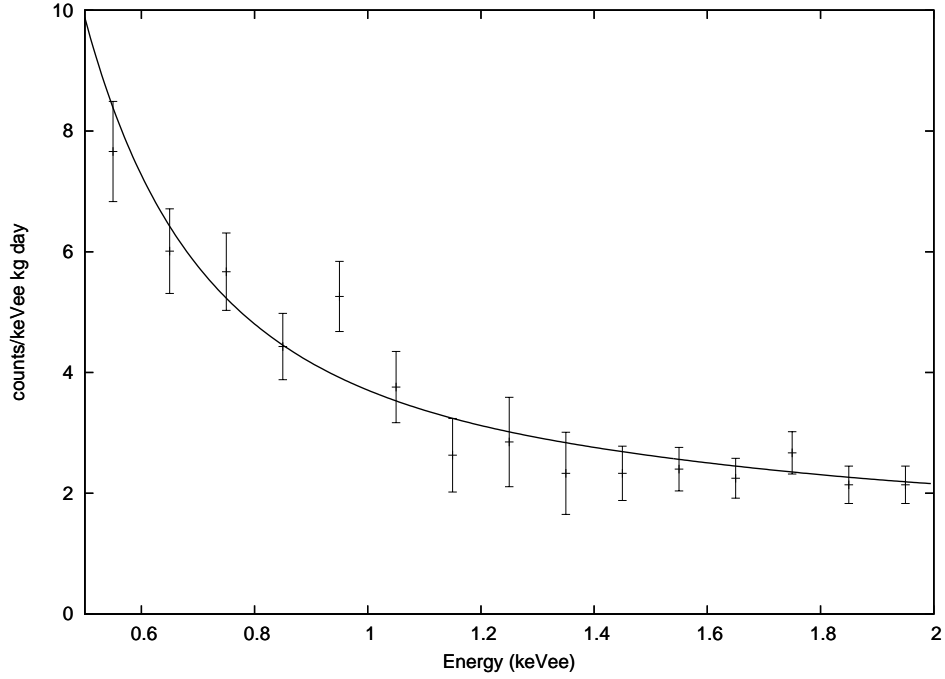


Figure 3b: CoGeNT spectrum for two component hidden sector dark matter with parameters  $P1$ . In this example  $q_{Ge} = 0.17$ .

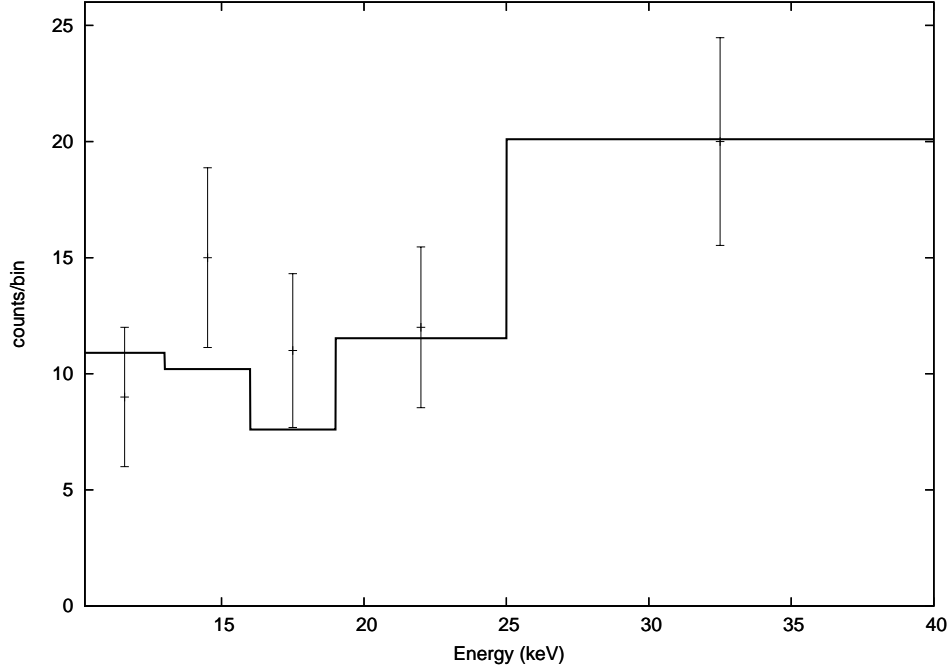


Figure 3c: CRESST spectrum for two component hidden sector dark matter for the example *P1*.

Figures 3 clearly demonstrates that two component hidden sector dark matter can simultaneously explain DAMA, CoGeNT and CRESST-II data. The apparent bump in the DAMA data can be reproduced extremely well and the minimal model predicts a change in sign of the DAMA annual modulation signal at low energies. Note though, that if there are additional particles,  $F_3$ , of intermediate mass  $\sim 20$  GeV, then their positive contribution to the annual modulation can outweigh the negative contribution from  $F_2$ . An example, given in the context of mirror dark matter with  $F_2 \sim Fe'$  and  $F_3 \sim O'$ , was discussed in ref.[12]. Figure 3b indicates that the shape of the CoGeNT spectrum is nicely consistent with the  $dR/dE_R \propto 1/E_R^2$  predicted from the energy dependence of the Rutherford cross section. The event rate is predicted to continue to rise as  $\sim 1/E_R^2$  as the recoil energy is reduced below the current CoGeNT threshold, until the threshold of a lighter component is reached, whereby the rate can jump even higher. These effects can be probed by TEXONO, C-4 and possibly other experiments.

Future data from DAMA, CoGeNT, CRESST-II and other experiments will obviously be able to constrain the parameter space within this hidden sector framework. As discussed recently[32], a particularly striking diurnal modulation signal should be observable for a detector located in the southern hemisphere, and perhaps even in the northern hemisphere at low latitudes, such as detectors in Jin-Ping underground laboratory. In the meantime, we must rely on annual modulation and spectrum data.

In figure 4 we give the total predicted spectrum for DAMA/LIBRA for the reference point, *P1*. Figure 4 also shows the ‘single hit’ event rate recorded in DAMA/LIBRA[3].

The figure indicates that the sharp rise in the predicted dark matter interaction rate could potentially be differentiated from the background if the DAMA threshold is lowered below 2 keVee. In figure 5 we show the predicted annual modulation spectrum for CoGeNT for the same reference point,  $P1$ . Clearly, the initial annual modulation amplitude measured by CoGeNT to be  $A \approx 0.46 \pm 0.17$  cpd/kg/keVee averaged over the energy range:  $0.5 < E(\text{keVee}) < 3.0$ , is much larger than that predicted by our example point. Also, we find that the annual modulation changes sign at low energies. This feature is not supported by CoGeNT's initial measurement. However the energy where the modulation changes sign can be reduced if the mass of  $F_2$  is lowered, which can alleviate this discrepancy. Alternatively, there can be an additional dark component,  $F_3$ , of mass  $\sim 20$  GeV. As discussed earlier in the context of DAMA, such a component can give a positive contribution to the annual modulation which can outweigh the negative contribution from  $F_2$ . Clearly future measurements of the annual modulation by CoGeNT, C-4, CDEX, and other experiments will be of crucial importance.

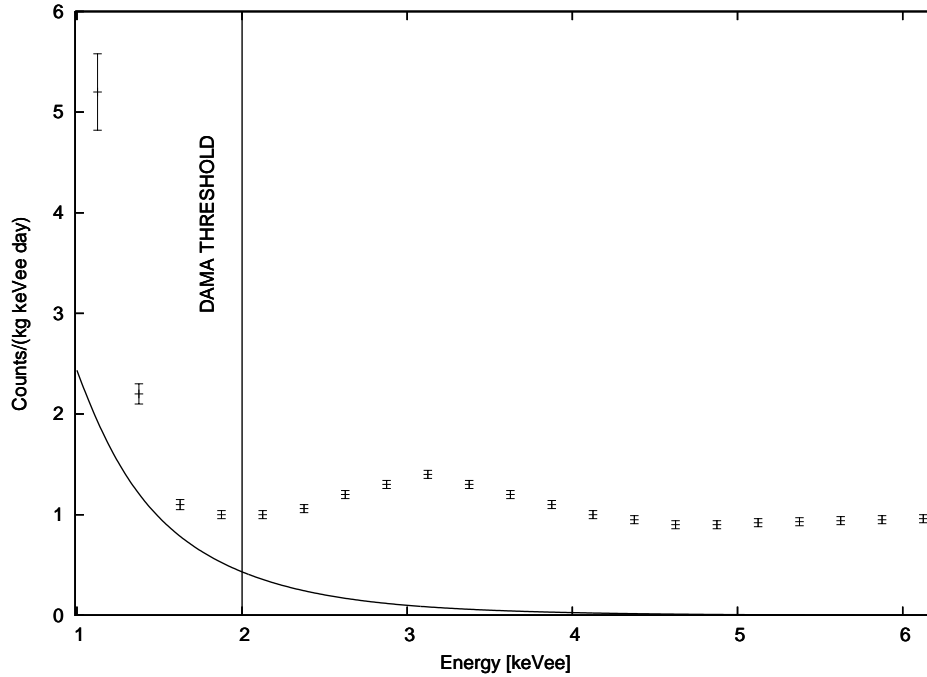


Figure 4: DAMA spectrum for hidden sector dark matter with parameters  $P1$ . In this example  $q_{Na} = 0.36$ ,  $q_I = 0.20$ .

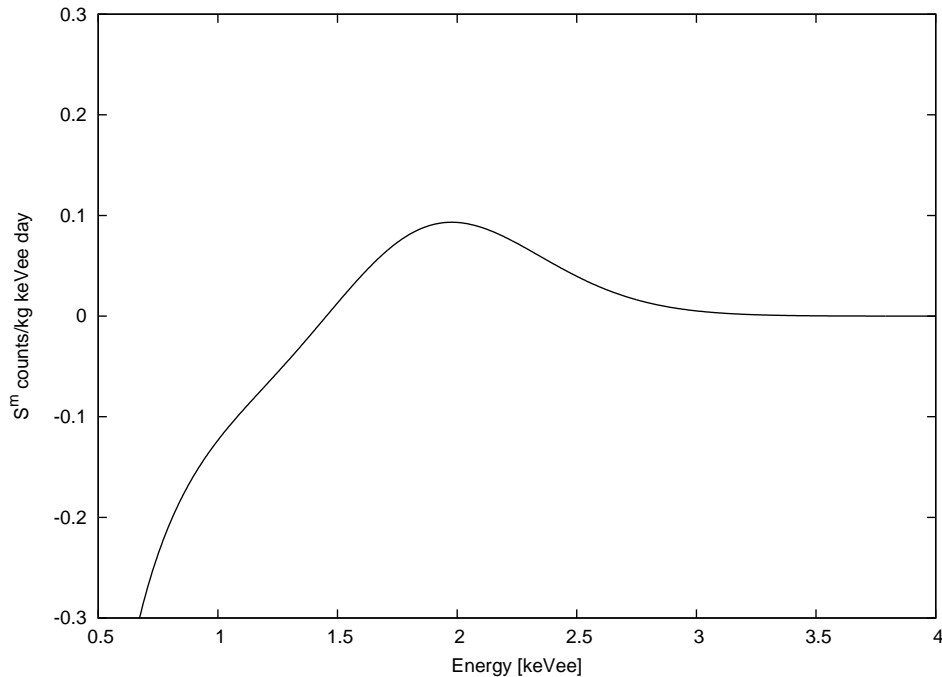


Figure 5: CoGeNT annual modulation spectrum for hidden sector dark matter with parameters  $P1$ . In this example  $q_{Ge} = 0.17$ .

## 6 Constraints from CDMS and XENON100

The CDMS/Ge[26], CDMS/Si[33] and XENON100[25] experiments have reported null results in their dark matter search. Here, we examine the compatibility of the considered hidden sector dark matter model with these null results <sup>7</sup>. The constraints from the CDMS and XENON100 experiments depend sensitively on the recoil energy threshold which (typically) has at least 20% uncertainty. The XENON100 experiment, which has the largest exposure, has particularly poor knowledge of energy calibration in the important low energy region (see ref.[38, 39] for some relevant discussions). Given this situation, we examine the compatibility issue by estimating the energy threshold for which the parameter point  $P1$  can be excluded at 95% C.L. We have taken into account the relevant detection efficiencies, exposure time etc, although we conservatively ignore effects of detector resolution for the XENON100 experiment. Our results are given in table 4. Note that the 95% C.L. limits in the second column arise since CDMS/Ge, CDMS/Si and XENON100 observed 2, 0, 2 events respectively in the low energy region.

---

<sup>7</sup>There are also lower threshold analysis by the XENON10[34] and CDMS collaborations[35]. However it has been argued[36] that neither analysis can exclude light dark matter (and by extension, hidden sector dark matter considered here, which has similar event rates at low energies) when systematic uncertainties are properly taken into account. Interestingly, a recent analysis[37] has found that the low energy CDMS data are actually fully consistent with CoGeNT's observed low energy excess rate, adding weight to the dark matter interpretation of this excess.



Experiment	95% C.L limit	$E_R^{est}$ threshold	$E_R^{nom}$ threshold	100	$1 - \frac{E_R^{nom}}{E_R^{est}}$
CDMS/Ge	6.3	12.8 keV	10.0 keV	22 %	
CDMS/Si	3.0	8.8 keV	7.0 keV	20 %	
XENON100	6.3	13.0 keV	6.6 keV	49 %	

Table 4: Estimated energy threshold ( $E_R^{est}$ ) for which the CDMS/Ge, CDMS/Si and XENON100 experiments are consistent with the hidden sector dark matter expectations assuming the example point,  $P1$ .  $E_R^{nom}$  is the nominal energy threshold of each experiment. The last column gives the percentage at which the energy threshold needs to have been underestimated for the point  $P1$  to be consistent with these experiments at 95% C.L.

Table 4 indicates that hidden sector dark matter with parameters given by the example  $P1$  is consistent with the CDMS/Ge, CDMS/Si [XENON100] data provided that the energy scale has been underestimated by of order 20% [50%]. This indicates that the hidden sector dark matter explanation of the DAMA, CoGeNT and CRESST-II experiments has some level of tension - especially with the XENON100 results. Our example point assumed  $\bar{m} = 1.0$  GeV. Raising  $\bar{m}$  will increase the tension of hidden sector dark matter with the null results of CDMS and XENON100 experiments. Lowering  $\bar{m}$  can improve the situation, but only moderately so, since  $\bar{m} = 1$  GeV is already very low. Although  $P1$  was just an example point, it seems that some level of tension exists between the null results of XENON100 and the hidden sector dark matter explanation of the DAMA, CoGeNT and CRESST-II experiments.

One can envisage several possible ways in which this tension might be alleviated. For example, it is possible that there is an issue with the calibration of the XENON100 apparatus. Determining the recoil energy scale in the XENON100 detector is nontrivial and it seems possible that this scale might be have a factor  $\sim 2$  uncertainty[38, 39]. Another possibility is that  $F_2$  has a somewhat lower mass than given in our example. This option would be especially relevant if we were to ignore the CRESST-II excess. For example the parameter point:

$$P2 : m_{F_2} = 40 \text{ GeV}, \epsilon\sqrt{\xi_{F_2}} = 5.7 \times 10^{-9}, \bar{m} = 1.0 \text{ GeV}, v_{rot} = 190 \text{ km/s} \quad (16)$$

yields a  $\chi^2(dama) = 18.9$  for 12 data points and  $\chi^2(cogent) = 22.8$  for 15 data points, but gives only around 1 event for the CRESST-II exposure. This is a reasonable fit for DAMA and CoGeNT, considering that the shape of the distributions are fit well, only the overall normalization is not [CoGeNT (DAMA) prefers slightly smaller (larger)  $\epsilon\sqrt{\xi_{F_2}}$ , with  $\epsilon\sqrt{\xi_{F_2}} = 5.7 \times 10^{-9}$  a compromise]. The different normalizations might easily be due to systematic effects not included in our analysis. In table 5 we estimate the energy threshold for which the CDMS/Ge, CDMS/Si and XENON100 experiments are consistent with hidden sector dark matter expectations assuming the example point  $P2$ .

Finally, the KIMS experiment[40] is currently operating with a  $\sim 100$  kg  $CsI$  target. Using a Pulse Shape Analysis (PSA), they have announced a ( $2\sigma$ ) limit on the rate of

Experiment	95% C.L limit	$E_R^{est}$ threshold	$E_R^{nom}$ threshold	100	$1 - \frac{E_R^{nom}}{E_R^{est}}$
CDMS/Ge	6.3	9.8 keV	10.0 keV	-2 %	
CDMS/Si	3.0	7.3 keV	7.0 keV	4 %	
XENON100	6.3	9.4 keV	6.6 keV	30 %	

Table 5: Same as Table 4, except for the parameter point  $P2$ .

dark matter interactions:  $R < 0.02$  cpd/kg/keVee for  $3 < E_R(\text{keVee}) < 4$ . We find that the predicted rate of Iodine interactions in a  $CsI$  target, for the parameter point  $P1$ , is  $R \approx 0.007$  cpd/kg/keVee in the  $3 < E_R(\text{keVee}) < 4$  bin and falls sharply at higher energies. [Assuming here the resolution and  $q_I$  quenching factor for KIMS are the same as in the DAMA/LIBRA experiment]. Thus, their PSA does not currently constrain hidden sector dark matter. However, the KIMS experiment also hopes to measure or constrain the annual modulation amplitude. These results are expected to be reported shortly. We note here that KIMS can potentially see a positive signal for a significant portion of parameter space (c.f. dashed-dotted line in figure 3a).

## 7 Conclusion

We have examined the data from the DAMA, CoGeNT and CRESST-II experiments in the context of multi-component hidden sector dark matter models. The models considered feature a hidden sector with two or more stable particles charged under an unbroken  $U(1)'$  gauge interaction. The new gauge field can interact with the standard  $U(1)_Y$  via renormalizable kinetic mixing, leading to Rutherford-type elastic scattering of the dark matter particles off ordinary nuclei. We considered the simplest generic model of this type, with a hidden sector composed of two stable particles,  $F_1$  and  $F_2$ .

We have found that the two component hidden sector dark matter model can simultaneously explain the DAMA, CoGeNT and CRESST-II data. This explanation is consistent with the null results of the CDMS/Si and CDMS/Ge experiments when  $\sim 20\%$  systematic uncertainties in energy scale are considered. There is some tension with the XENON100 experiment. The favoured parameter regions are typically consistent with the most recent XENON100 results only if the XENON100 energy threshold is around a factor of two higher than given by the XENON100 collaboration.

## Acknowledgments

This work was supported by the Australian Research Council.

## References

- [1] S. Dodelson, “Modern cosmology,” Amsterdam, Netherlands: Academic Pr. (2003) 440 p; G. Bertone, D. Hooper and J. Silk, Phys. Rept. **405**, 279 (2005)

[hep-ph/0404175].

- [2] R. Bernabei *et al.* [DAMA Collaboration], Riv. Nuovo Cimento. **26**, 1 (2003) [astro-ph/0307403]; Int. J. Mod. Phys. E**13**, 2127 (2004); Phys. Lett. B**480**, 23 (2000).
- [3] R. Bernabei *et al.* [DAMA Collaboration], Eur. Phys. J. C**56**, 333 (2008) [arXiv:0804.2741]; Eur. Phys. J. C**67**, 39 (2010) [arXiv: 1002.1028].
- [4] A. K. Drukier, K. Freese and D. N. Spergel, Phys. Rev. D**33**, 3495 (1986); K. Freese, J. A. Frieman and A. Gould, Phys. Rev. D**37**, 3388 (1988).
- [5] C. E. Aalseth *et al.* [CoGeNT Collaboration], Phys. Rev. Lett. **106**, 131301 (2011) [arXiv:1002.4703]; Phys. Rev. Lett. **107**, 141301 (2011) [arXiv:1106.0650].
- [6] C. E. Aalseth *et al.* [CoGeNT Collaboration], arXiv:1208.5737.
- [7] G. Angloher, M. Bauer, I. Bavykina, A. Bento, C. Bucci, C. Ciemniak, G. Deuter and F. von Feilitzsch *et al.*, arXiv:1109.0702.
- [8] R. Foot, Phys. Rev. D**69**, 036001 (2004) [hep-ph/0308254].
- [9] R. Foot, Mod. Phys. Lett. A**19**, 1841 (2004) [astro-ph/0405362]; astro-ph/0403043; Phys. Rev. D**74**, 023514 (2006) [astro-ph/0510705]; Phys. Rev. D**82**, 095001 (2010) [arXiv: 1008.0685]; Phys. Lett. B**692**, 65 (2010) [arXiv: 1004.1424].
- [10] R. Foot, Phys. Rev. D**78**, 043529 (2008) [arXiv: 0804.4518].
- [11] R. Foot, Phys. Lett. B **703**, 7 (2011) [arXiv:1106.2688].
- [12] R. Foot, Phys. Rev. D **86**, 023524 (2012) [arXiv:1203.2387].
- [13] R. Foot, H. Lew and R. R. Volkas, Phys. Lett. B **272**, 67 (1991); Mod. Phys. Lett. A **7**, 2567 (1992).
- [14] R. Foot, Int. J. Mod. Phys. D**13**, 2161 (2004) [astro-ph/0407623]; Int. J. Mod. Phys. A**19** 3807 (2004) [astro-ph/0309330]; P. Ciarcelli, Int. J. Mod. Phys. D**19**, 2151 (2010) [arXiv: 1102.5530].
- [15] J. -W. Cui, H. -J. He, L. -C. Lu and F. -R. Yin, Phys. Rev. D **85**, 096003 (2012) [arXiv:1110.6893].
- [16] J. L. Feng, H. Tu and H. -B. Yu, JCAP **0810**, 043 (2008) [arXiv:0808.2318]; J. L. Feng, M. Kaplinghat, H. Tu and H. -B. Yu, JCAP **0907**, 004 (2009) [arXiv:0905.3039].
- [17] N. F. Bell, K. Petraki, I. M. Shoemaker and R. R. Volkas, Phys. Rev. D **84**, 123505 (2011) [arXiv:1105.3730]; K. Petraki, M. Trodden and R. R. Volkas, JCAP **1202**, 044 (2012) [arXiv:1111.4786] and references there-in.

- [18] N. Fornengo, P. Panci and M. Regis, Phys. Rev. D **84**, 115002 (2011) [arXiv:1108.4661].
- [19] R. Foot and X-G. He, Phys. Lett. B **267**, 509 (1991).
- [20] B. Holdom, Phys. Lett. B **166**, 196 (1986).
- [21] R. H. Helm, Phys. Rev. **104**, 1466 (1956).
- [22] J. D. Lewin and P. F. Smith, Astropart. Phys. **6**, 87 (1996).
- [23] R. Foot and R. R. Volkas, Phys. Rev. D **70**, 123508 (2004) [astro-ph/0407522].
- [24] J. M. Cline, Z. Liu and W. Xue, Phys. Rev. D **85**, 101302 (2012) [arXiv:1201.4858].
- [25] E. Aprile *et al.* [XENON100 Collaboration], arXiv:1207.5988.
- [26] Z. Ahmed *et al.* [CDMS-II Collaboration], Science **327**, 1619 (2010) [arXiv:0912.3592].
- [27] N. Bozorgnia, G.B. Gelmini and P. Gondolo, JCAP **1011**, 019 (2010) [arXiv: 1006.3110]; JCAP **1011**, 028 (2010) [arXiv: 1008.3676].
- [28] A. Brunthaler, M. J. Reid, K. M. Menten, X. -W. Zheng, A. Bartkiewicz, Y. K. Choi, T. Dame and K. Hachisuka *et al.*, arXiv:1102.5350.
- [29] M. T. Frandsen, F. Kahlhoefer, C. McCabe, S. Sarkar and K. Schmidt-Hoberg, JCAP **1201**, 024 (2012) [arXiv:1111.0292].
- [30] R. Bernabei *et al.* [DAMA Collaboration], Nucl. Instrum. Meth. A **592**, 297 (2008) [arXiv:0804.2738].
- [31] V. I. Tretyak, Astropart. Phys. **33**, 40 (2010) [arXiv:0911.3041].
- [32] R. Foot, JCAP **1204**, 014 (2012) [arXiv:1110.2908].
- [33] J. P. Filippini, Ph. D. thesis (2008).
- [34] J. Angle *et al.* (XENON10 Collaboration), arXiv: 1104.3088.
- [35] Z. Ahmed *et al.* (CDMS Collaboration), Phys. Rev. Lett. **106**: 131302 (2011) [arXiv: 1011.2482].
- [36] J. I. Collar, arXiv:1103.3481; arXiv:1106.0653.
- [37] J. I. Collar and N. E. Fields, arXiv:1204.3559.
- [38] J. I. Collar, arXiv:1010.5187.
- [39] R. Cerulli *et al.*, arXiv:1201.4582.
- [40] S. K. Kim, on behalf of the KIMS collaboration, TAUP 2011 workshop, Munich, Germany Sep 5-9, 2011.